Research Article

Solution-Processable Quinoidal Dithioalkylterthiophene-Based Small Molecules Pseudo-Pentathienoacenes *via* an Intramolecular S···S Lock for High-Performance n-Type Organic Field-Effect Transistors

Sureshraju Vegiraju,[¶] Alfonsina Abat Amelenan Torimtubun,[¶] Po-Shen Lin, Hsin-Chia Tsai, Wei-Chieh Lien, Cheng-Shiun Chen, Guan-Yu He, Chih-Yu Lin, Ding Zheng, Yi-Fan Huang, Yi-Ching Wu, Shueh-Lin Yau, Gene-Hsiang Lee, Shih-Huang Tung, Chien-Lung Wang, Cheng-Liang Liu,* Ming-Chou Chen,* and Antonio Facchetti*

Cite This: *ACS Appl. Mater. Interfaces* 2020, 12, 25081−25091

Read Online

ACCESS | Metrics & More | Article Recommendations | Supporting Information

ABSTRACT: A new organic small-molecule family comprising tetracyanoquinodimethane-substituted quinoidal dithioalky(SR)terthiophenes (**DSTQ**s) (**DSTQ-6** (**1**); SR = SC_6H_{13}, **DSTQ-10** (**2**); SR = $SC_{10}H_{21}$, **DSTQ-14** (**3**); SR = $SC_{10}H_{21}$) was synthesized and contrasted with a nonthioalkylated analogue (**DRTQ-14** (**4**); R = $C_{14}H_{29}$). The physical, electrochemical, and electrical properties of these new compounds are thoroughly investigated. Optimized geometries obtained from density functional theory calculations and single-crystal X-ray diffraction reveal the planarity of the SR-containing **DSTQ** core. **DSTQ**s pack in a slipped $\pi-\pi$ stacked two-dimensional arrangement, with a short intermolecular stacking distance of 3.55 Å and short intermolecular S···N contacts of 3.56 Å. Thin-film morphological analysis by grazing incident X-ray diffraction reveals that all **DSTQ** molecules are packed in an edge-on fashion on the substrate. The favorable molecular packing, the high core planarity, and very low lowest unoccupied molecular orbital (LUMO) energy level (−4.2 eV) suggest that **DSTQ**s could be electron-transporting semiconductors. Organic field-effect transistors based on solution-sheared **DSTQ-14** exhibit the highest electron mobility of 0.77 $cm^2 V^{-1} s^{-1}$ with good ambient stability, which is the highest value reported to date for such a solution process terthiophene-based small molecular semiconductor. These results demonstrate that the device performance of solution-sheared **DSTQ**s can be improved by side chain engineering.

KEYWORDS: *dithioalkylterthiophene, quinoidal, pseudo-pentathienoacenes, organic field-effect transistors, tetracyanoquinodimethane*

1. INTRODUCTION

Solution processable π-conjugated organic small molecules have attracted much attention for their potential applications in, among others, organic field-effect transistors (OFETs), which can be used to fabricate memory devices, smart cards, radio frequency identification tags, electronic papers, flexible displays, and sensors.[1−11] Most of these devices require two charge carrying-type OFETs, one which transports holes (p-channel) and one which transports electrons (n-channel). The design of these solution-processed small molecules are composed of a planar conjugated building blocks with suitable solubilizing alkyl side chains. The inter/intramolecular interactions, molecular packing, and device performances can be significantly affected by the modifications of these alkyl side chains.[12−15] The development of solution-processable n-channel OFETs based on small molecular organic semiconductors has made substantial progress during the past decade.[16−19] The most prominent examples consist of

electron-poor building blocks such as tetraazapentacenes, diketopyrrolopyrrole (**DPP**),[20,21] naphthalenediimides (**NDIs**),[22−24] perylenecarboxydiimide (**PDI**),[25] and other oligo/fused thiophene[26−28] based cores optionally functionalized with electron-withdrawing functionalities such as perfluorophenyls,[29] cyano,[30] and alkyl cyanoacetates.[17] Among several examples of conjugated n-channel small molecules, tetracyanoquinodimethane (**TQ**)-containing molecules (see examples in Figure 1)[31−35] have shown good electron transport in ambient, thanks to their low lowest unoccupied molecular orbital (LUMO) energy and strong
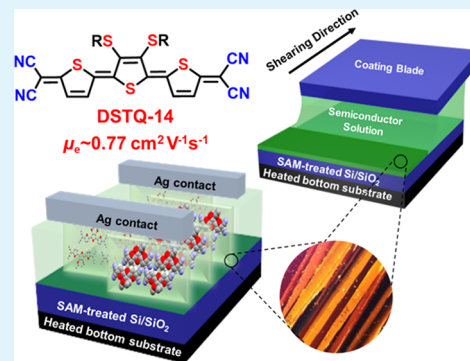
a)

DCMT (I)
$\mu_{e(v)}$: 0.2 cm²V⁻¹s⁻¹(R=C₄H₉)

II
$\mu_{e(s)}$: 0.16 cm²V⁻¹s⁻¹ (R=C₆H₁₃)

TTTCN (III)
$\mu_{e(s)}$: 0.05 cm²V⁻¹s⁻¹(R=C₈H₁₇)

3T (IV)
$\mu_{e(s)}$: 0.007 cm²V⁻¹s⁻¹(R=C₆H₁₃)

b)

DSTQ
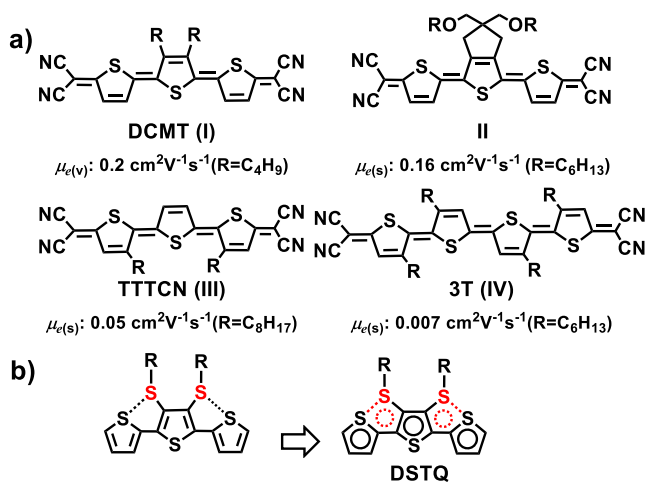
Figure 1. (a) Chemical structures of the reported oligothiophene-based quinoidal dicyanomethylene substituted n-type small molecules. The symbols (v) and (s) denote semiconductor films of vacuum and solution processes. (b) Pseudo-pentathienoacene-like structure of **DSTQ**.

electron affinity. Besides the low-lying LUMO (<−3.9 eV), the tetracyanoquinodimethane unit can also be linked synthetically to most known conjugated building blocks to convert them to a potential n-type semiconductor.[36−44] Despite these promises, **TQ**s have not outperformed other high-performance n-channel organic semiconductor families, which is probably due to the very limited extension of the π-core and molecular disorder as the result of the different diastereoisomers in **TQ** oligothiophenes.[17,27] Among the best examples, vacuum-deposited **DCMT** (**I**) exhibited the highest electron mobility of ∼0.2 cm² V⁻¹ s⁻¹[35] and solution-deposited films of **II** were reported with an electron mobility of 0.16 cm² V⁻¹ s⁻¹.[34]

The introduction of sidechains into π-conjugated molecular/polymeric backbones not only enables their thin-film processing from solution but also plays an important role in tuning their solid-state optical and electronic properties. Over the past few years, a few polymers have been functionalized with thioalkyl chains to improve their photovoltaic performances.[45−47] In addition, we have recently developed soluble dithioalkyl-substituted bithiophene-based semiconductors, in which the sulfur atoms in the thioalkyl chains provide intramolecular locks with the other sulfur atoms in the thiophene (S···S), which enhances the molecular planarity and hole mobility.[48−51] Thus, an interesting question is whether this approach could promote more structurally ordered **TQ**s and promote intermolecular forces and electron mobility.

In this report, using the above strategy, we used different thioalkyl side chains to synthesize tetracyanoquinodimethane-substituted quinoidal dithioalkylterthiophene (**DSTQ**s) resulting in new compounds **DSTQ-6** (**1**; SR = SC₆H₁₃), **DSTQ-10** (**2**; SR = SC₁₀H₂₁), **DSTQ-14** (**3**; SR = SC₁₄H₂₉). A nonthioalkylated derivative, **DRTQ-14** (**4**; R = C₁₄H₂₉), was also synthesized for comparison. We systematically investigated the effect of the (thio)alkyl side chain substitution on the terthiophene core on molecular and thin-film properties as well as charge transport in OFET devices. Semiconductor film deposition optimization was carried out by semiconductor processing using solution-shearing methods versus conventional spin-coating. Thus, OFETs' performance and thin-film morphology were investigated as a function of processing

demonstrating the superiority of shearing to enhance molecular order and carrier mobility. In particular, quinoidal **DSTQ-14**, which has a dithiotetradecyl side chain, exhibits the highest OFET electron mobility of 0.77 cm² V⁻¹ s⁻¹ of the series. Morphological and structural analyses revealed that the improved mobility is due to high crystallinity caused by the high degree of interchain ordering and π−π stacking propensity. Our data suggested that this new **DST**-heteroarene molecular design, enabling pseudo-fused pentathienoacene structures (Figure 1b), affords highly soluble, yet considerably planarized, molecular semiconductors for optoelectronics.

2. RESULTS AND DISCUSSION

2.1. Synthesis. The synthetic route to quinoids **1−4** is shown in Scheme 1. The central dithioallylated thiophene (**7**)

Scheme 1. Synthetic Route to Quinoidal Semiconductors 1−4

1: **DSTQ-6**; (S)R = SC₆H₁₃
2: **DSTQ-10**; (S)R = SC₁₀H₂₁
3: **DSTQ-14**; (S)R = SC₁₄H₂₉
4: **DRTQ-14**; (S)R = C₁₄H₂₉
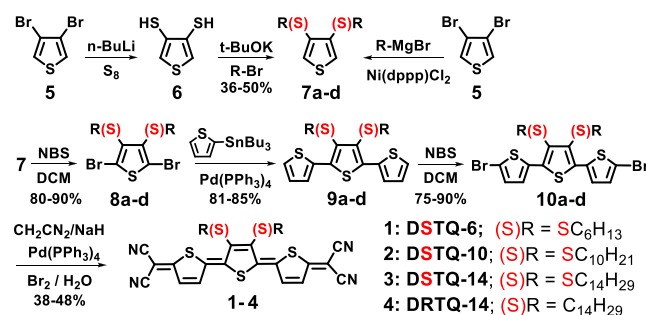
unit was prepared starting from 3,4-dibromothiophene (**5**), which was first dilithiated using *n*-BuLi, followed by the reaction with sulfur, and was then dialkylated with the corresponding alkyl bromide to afford **7**. However, the dialkylated thiophene analog (**7**) was prepared *via* a Kumada coupling of **5** with the corresponding alkyl Grignard reagent catalyzed by the Nickel complex.[52] After dibromination of molecules **7** with *n*-bromosuccinimide (NBS) to give the corresponding **8**, it was then coupled with 2-(tributylstannyl)-thiophene in the presence of a palladium catalyst to give dithiophenylthiophenes **9**. Again, upon treatment of the latter with NBS, the dibrominated terthiophenes **10** were prepared. *Via* Takahashi coupling of the latter with malononitrile in the presence of tetrakis(triphenylphosphine)palladium, followed by oxidation using a saturated solution of bromine in water, quinoids **DSTQ** (**1−3**) and **DRTQ** (**4**) were achieved. Most of the newly developed quionoids are well soluble in common organic solvents and suitable for thin-film solution-processing. All compound chemical structures were characterized by ¹H and ¹³C NMR, mass spectrometry. Furthermore, single-crystal X-ray analyses of **DSTQ-14** (**3**) and **DRTQ-14** (**4**) were obtained for comparison. Synthetic procedure details and characterization data are provided in the Supporting Information.

2.2. Physical Characterization. Thermal analyses of the new organic semiconductors were performed using differential scanning calorimetry (DSC: Figure S1) and thermogravimetric analysis (TGA; Figure S2), and the corresponding thermal data are summarized in Table 1. As revealed by the DSC scans, all compounds possess high melting points with sharp endotherms above 195 °C. From the TGA measurements, it can be seen that all four molecules exhibited high thermal stability with 5% weight loss at temperatures up to 260 °C

Table 1. Thermal, Optical, and Electrochemical Properties of all Four Compounds

Compound	$T_d{}^a$ [°C]	$T_m{}^b$ [°C]	λ_{max} (soln)^c [nm]	λ_{max} (film)^d [nm]	$E_{ox}{}^e$ [V]	HOMO^f [eV]	$E_{red}{}^e$ [V]	LUMO^f [eV]	$\Delta E_g{}^g$ [eV]
1	267	208	695	675/720	1.43	−5.63	0.08	−4.28	1.35
2	296	212	695	677/725	1.43	−5.63	0.08	−4.27	1.36
3	310	202	695	675/720	1.42	−5.62	0.08	−4.28	1.34
4	393	195	680	655/705	1.41	−5.61	−0.02	−4.18	1.43

^{a}Decomposition temperatures were determined from TGA. ^{b}Melting temperatures were determined from DSC. ^{c}Absorption spectra were measured in o-$C_6H_4Cl_2$. ^{d}Thin films were solution-sheared onto a quartz glass. ^{e}By DPV in o-$C_6H_4Cl_2$ at 25 °C. All potentials are reported with reference to an Fc^+/Fc internal standard (at +0.6 V). ^{f}Using HOMO/LUMO = $-(4.2 + E_{ox}/E_{red})$. ^{g}The energy gap was calculated from the difference between HOMO and LUMO measured by DPV.[58]
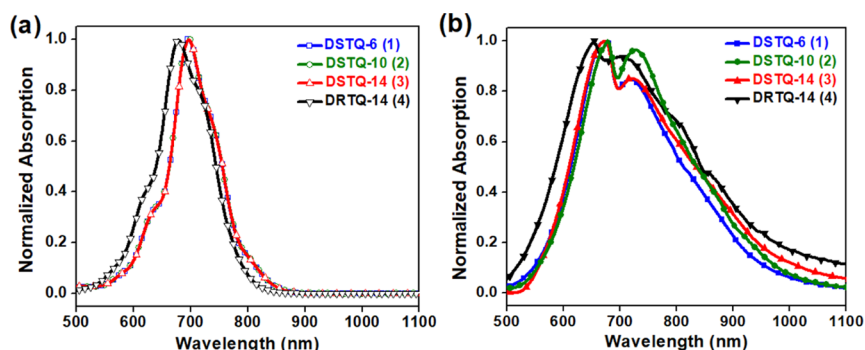
Figure 2. (a) Absorption spectra of all four compounds in diluted o-dichlorobenzene solution; (b) normalized absorption of solution-sheared film.
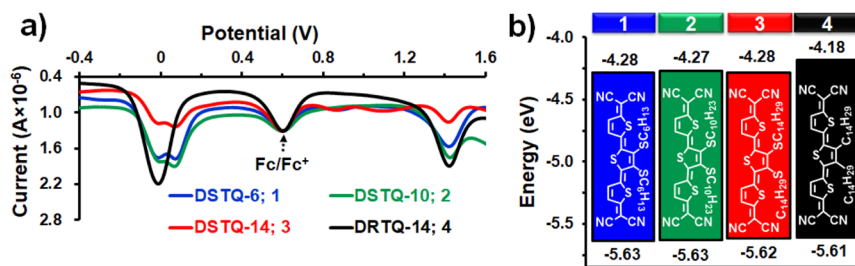
Figure 3. (a) DPV of **DSTQ**s in o-dichlorobenzene. (b) DPV-derived HOMO and LUMO energy levels.

(under nitrogen). **DRTQ-14** exhibited the highest thermal stability up to 393 °C. It is interesting to note that the thermal decomposition of all four molecules (**1−4**) is the result of two alkyl chains cleavage, as confirmed by the TGA weight loss profile.

The optical properties of **1−4** were measured by UV−vis spectroscopy both in chlorobenzene solution and as thin films prepared by solution-shearing (*vide infra*). As shown in Figure 2a, the solution absorption spectra of **DSTQ-6** (**1**), **DSTQ-10** (**2**), and **DSTQ-14** (**3**) are identical with maximum absorption band at 695 nm, indicating that the variation of thioalkyl side chain length does not lead to fundamental changes in the intrinsic electronic structure of the π-conjugated dithioterthiophene (**DST**) backbone. On the other hand, by comparing the absorption of **DRTQ-14** (**4**; λ_{max} (soln) at 680 nm), the introduction of the sulfur atom into the alkyl side moiety leads to significant bathochromic shift of ~15 nm. The thin-film spectra of **DSTQ-6**, **DSTQ-10**, **DSTQ-14**, and **DRTQ-14** are broad and contain a combination of blue-shifted and red-shifted features versus the solution spectra (Figure 2b), which can be explained by the thin-film H-type and J-type aggregation intermolecular aggregation, respectively. Apparently, the thioalkyl side chain length of **DSTQ** compounds do not influence the band gap too much. However, all **DSTQ**-based compounds exhibit a shoulder peak at ~720 nm, which

is attributed to J-type aggregation. The extent of aggregation, and thus the intensity of this band, is known to depend on several factors including (small) variations in packing motifs, intermolecular distances, intermolecular geometries, crystallite size, extent of crystalline versus amorphous aggregates to cite just a few of them.[53−55] Furthermore, the typical Davydov splitting indicated by both high-energy and low-energy transition can be easily observed in the optical properties of thiophene-based oligomers and quinoidal molecules with dicyanomethylene groups attached in conjugated backbone.[27,31,56,57]

Differential pulse voltammetry (DPV) was employed to examine the electrochemical properties of **1−4** in o-dichlorobenzene with a 0.1 M Bu_4NPF_6 solution at 25 °C. The DPV curves and the corresponding highest occupied molecular orbital (HOMO) and the lowest unoccupied molecular orbital (LUMO) energy levels are presented in Figure 3 and the data are listed in Table 1. The LUMO energies of all three **DSTQ**s are below −4.2 eV, which are sufficiently deep enough for efficient electron injection and ambient stable electron transport, thus enabling the potential application as ambient-stable n-type organic semiconductors. It is found that modifying the length of the alkyl side chain does not influence the electrochemical properties of **DSTQ**s. In contrast, the HOMO/LUMO energy levels are obviously
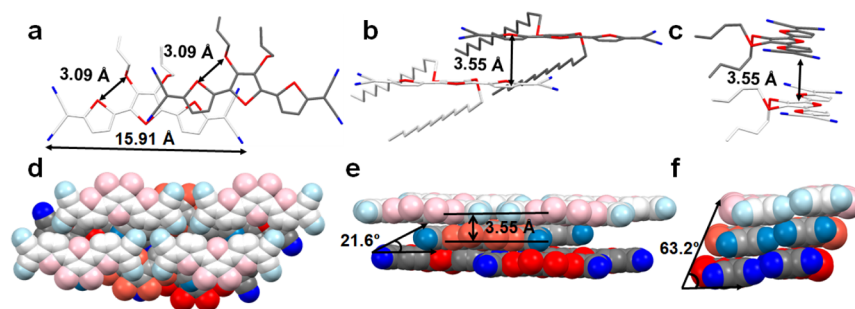
Figure 4. Single-crystal structure of **DSTQ-14** (**3**) in stick models (a−c) and space filling packing models (d−f). (a) Top view of **3** with intramolecular S−S distance of 3.09 Å and the molecular length of 15.9 Å. (b) Front view of two stacking **DSTQ** molecules. The interplanar distance is ∼3.55 Å. (c) Side view of **3**. (d−f) Molecular packing arrangement of **DSTQ** with a face-to-face layer stacking distance of 3.55 Å and exhibition of the slipping angles of 21.61 and 63.2°. The red (and light red), blue (and light blue), and gray (and light gray) colored balls indicate sulfur, nitrogen, and carbon atoms, respectively. Alkyl side chains are partially omitted for clarity.
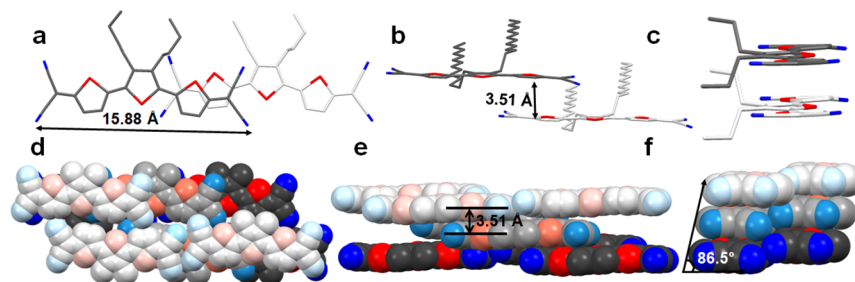
Figure 5. Single-crystal structure of **DRTQ-14** (**4**) in stick models (a−c) and space filling packing models (d−f). (a) Top view of **4**. (b) Front view of two stacking **DRTQ** molecules. The interplanar distance is ∼3.51 Å. (c) Side view of **4**. (d−f) Molecular packing arrangement of **DRTQ** with a face-to-face layer stacking distance of 3.51 Å and exhibition of the slipping angles of 22 and 86.5°. The red (and light red), blue (and light blue), and gray (and light gray) colored balls indicate sulfur, nitrogen, and carbon atoms, respectively. Alkyl side chains are partially omitted for clarity.

affected by introducing the sulfur atom into the alkyl side chain moieties, which provides deeper LUMO (−4.28/−4.27 eV for **DSTQs** vs −4.18 eV for **DRTQ-14**) and HOMO (−5.63/−5.62 eV for **DSTQs** vs −5.61 eV for **DRTQ-14**) energies. This result indicates that the **DSTQ** framework with sulfur introduced in the alkyl side chains could stabilize electron transport compared to their conventional alkylated analog. Furthermore, it is worth noting that the LUMO energy level of **DSTQs** closely approaches the work function of silver electrodes (−4.26 eV), which may facilitate charge injection and thereby enhance electron mobility. Besides that, the electrochemically derived HOMO−LUMO energy gaps of all **DSTQs** are ∼1.35 eV. This small band gap (E_g) suggests that **DSTQs** are favorable as a new type of semiconducting material.

To gain further insight into the effect of side chain engineering on the electronic structure and molecular geometry of four quinoidal compounds, density functional theory (DFT) calculations were performed at the B3LYP/6-31G* level of the Gaussian 03W program. All of the calculated compounds show similar electron density distribution for HOMO and LUMO along the entire quinoidal backbone (Figure S3). This electron density distribution demonstrated a significant delocalization of the quinoidal structure. Furthermore, a down-shifted tendency is also observed in the calculated HOMO and LUMO energy levels of **DSTQ-6**, **DSTQ-10**, and **DSTQ-14** compared to **DRTQ-14**, indicating that the introduction of sulfur atoms in the alkyl side moiety plays a role in affecting the electronic structures of the **DSTQ** conjugated core and is consistent with the DPV experimental results. Specifically, the calculated LUMO of all **DSTQs**

compounds is ∼−4.30 eV, indicating that the selection of suitable thioalkyl side chain leads to the possibility for the potential environmentally stable OFETs. The optimized geometries obtained from DFT calculations (Figure S4) suggest that the **DSTQ** conjugated cores are highly planar, which would promote an efficient delocalization of the π-electrons and facilitate π−π overlap and intermolecular interactions; therefore, it could be beneficial for charge transport. In particular, the inter-ring torsion angle between thiophene units of **DSTQ-6**, **DSTQ-10**, and **DSTQ-14** (2.71−2.89°) is about one-half the value of **DRTQ-14** (5.17°), indicating that thioalkyl introduction could favor planarity of the conjugated core, which allows to better charge transport efficiency.

2.3. Single-Crystal Structure. Single crystals of **DSTQ-14** and **DRTQ-14** were grown in a mixture of hexanes and dichloromethane by slow solvent evaporation in order to gain further insight into their molecular packing pattern and charge-transport properties. Their molecular structure and the complete crystal data derived from X-ray crystallographic analysis are shown in Figures 4 and 5. Both the **DSTQ-14** and **DRTQ-14** crystallized in the triclinic space group of P1 (for crystal data Tables S1 and S2) and adopted face-to-face slipped π−π stacking arrangement with a stacking distance of 3.55, 3.51 Å and layer slipping angle of 21.61, 22°, respectively. This face-to-face stacking of the π-stacking structure is believed to be more efficient for charge transport. The shortest intermolecular distances between S(thiophene)···N and S···S (between thiophenes) are 3.56 and 3.93 Å for **DSTQ-14**, 3.63 and 3.75 Å for **DRTQ-14**. In particular, the shortest intermolecular N···H distances among the face-to face layers
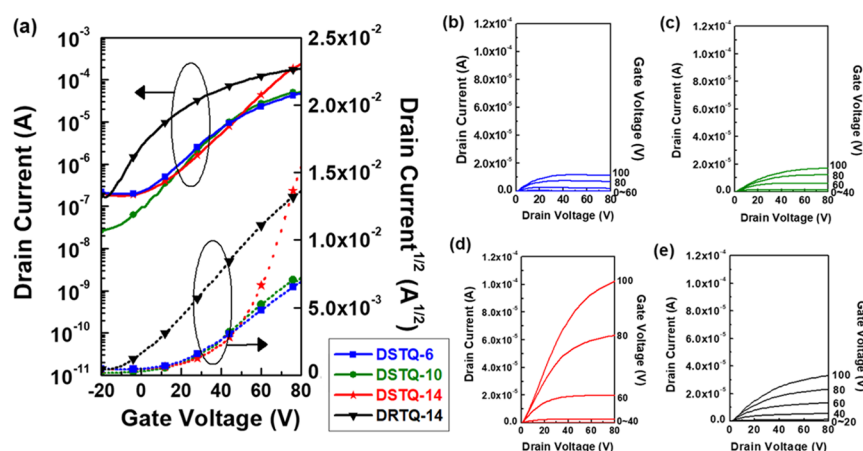
Figure 6. Representative transfer characteristics of solution-sheared OFETs based on (a) all four thin films (under a constant V_d of 80 V). Output characteristics of solution-sheared OFETs based on (b) **DSTQ-6**, (c) **DSTQ-10**, (d) **DSTQ-14**, and (e) **DRTQ-14** thin films. All the OFETs were measured in air at room temperature.

Table 2. Summary of OFET Parameters Based on Solution-Sheared and Spin-Coated DSTQ Thin Films, as Measured in Air at Room Temperature

	solution-sheared film				spin-coated film			
Compound	$\mu_{max}{}^a$ [cm^2 V^{-1} s^{-1}]	$\mu_{avg}{}^b$ [cm^2 V^{-1} s^{-1}]	$V_{th}{}^b$ [V]	I_{ON}/I_{OFF} [−]	$\mu_{max}{}^a$ [cm^2 V^{-1} s^{-1}]	$\mu_{avg}{}^b$ [cm^2 V^{-1} s^{-1}]	$V_{th}{}^b$ [V]	I_{ON}/I_{OFF} [−]
1	0.045	0.031 ± 0.014	32 ± 2.4	10^2 to 10^3	0.0002	0.00010 ± 0.00007	5.2 ± 0.7	10^1 to 10^2
2	0.064	0.053 ± 0.008	20 ± 3.6	10^3 to 10^4	0.04	0.037 ± 0.001	10 ± 1.7	10^2 to 10^3
3	0.77	0.56 ± 0.07	36 ± 2.3	10^3 to 10^4	0.064	0.055 ± 0.009	5 ± 2.6	10^2 to 10^3
4	0.14	0.09 ± 0.02	12 ± 6.7	10^3 to 10^4	0.042	0.04 ± 0.01	15 ± 2.7	10^2 to 10^3

[a]Maximum mobility. [b]The average TFT characteristics were obtained from more than 10 devices originating from 3 to 4 semiconductor depositions.

of **DSTQ-14** molecules are 2.51−2.53 Å (Figure S5), which are much shorter than those in **DRTQ-14** (2.66−2.71 Å, Figure S6). These intermolecular interactions in both **DSTQ-14** and **DRTQ-14**, along with $\pi-\pi$ interactions, formed two-dimensional networks in the crystals, which facilitate charge transport. Both quinoids are quite planar with small distortional angles and thus are expected to be good candidates for OTFTs. It is worth noting that an intramolecular nonbonded contact between the sulfur atom in the central thiophene ring and sulfur atom in alkyl side moieties exists in **DSTQ-14** (3.09 Å), which is shorter than twice the van der Waals radius of the S atom (3.70 Å).[51]

2.4. Charge-Transport Measurements. To investigate the effects by sulfur atom introduction and different alkyl substituent lengths in the side chain of **DSTQs** on OFET performance, bottom-gate top-contact devices were fabricated by solution-shearing and, in control devices, by spin-coating methods.[59−64] Solution-shearing was preferred to achieve aligned crystalline semiconductor domains having favorable charge-transport characteristics by controlling the semiconductor film morphology. Film optimization can be carried out by varying solution-shearing process parameters such as shearing speed, substrate temperature, as well as semiconductor concentration. All the devices, which were fabricated and measured under ambient conditions, exhibit n-type charge-transport characteristics, probably as a result of the deep LUMO energy levels. Particular devices were stored in the air for further ambient stability measurements. Silver was used for the electrodes mainly because of the close value between Ag work function (−4.26 eV) and the LUMO value of **DSTQ**s, leading to good charge carrier injection. Figure 6

depicts the representative OFET transfer and output curves. The transfer characteristics (I_d-V_g: drain current−gate voltage) in Figure 6a clearly show only n-type field-effect behavior as the result of the low-lying LUMO energy level. As shown in Figure 6b−e, their output characteristic (I_d-V_d: drain current−drain voltage) ranging from 0 to 80 V presents a well-fitted linear and saturation regime for good OFETs' performance. The electron mobilities (μ) and threshold voltage (V_{th}) were extracted from the slope and intercept of I_d versus V_g in the saturation regime.

The device performance, including maximum mobility (μ_{max}), average mobility (μ_{avg}), V_{th}, and current ON/OFF ratios (I_{ON}/I_{OFF}) are summarized in Table 2. The results show that there is a mobility dependence on the thioalkyl side chain length. OFETs based on **DSTQ-6** and **DSTQ-10** displayed electron mobilities of 0.031 ± 0.014 cm^2 V^{-1} s^{-1}; 0.053 ± 0.008 cm^2 V^{-1} s^{-1} (μ_{avg}) and 0.045 cm^2 V^{-1} s^{-1}; 0.064 cm^2 V^{-1} s^{-1} (μ_{max}), respectively, which thus slightly increases when the thioalkyl side chain length increases from thio-hexyl to thio-decyl. The slightly higher I_{ON}/I_{OFF} of these two molecules showed a similar tendency behavior correlated with the mobility and the side chain length. However, the μ_{max} of **DSTQ-14**-based OFET devices improves dramatically to the highest value of 0.77 cm^2 V^{-1} s^{-1} (μ_{avg} of 0.56 ± 0.07 cm^2 V^{-1} s^{-1}), thus for the longest thio-tetradecyl chain. **DSTQ-14** not only displayed an improved mobility but also a respectable I_{ON}/I_{OFF} of up to ~10^4, indicating good current modulation characteristics. One notable characteristic is that the **DRTQ-14** gives a lower mobility (μ_{max} = 0.14 cm^2 V^{-1} s^{-1}; μ_{avg} = 0.09 ± 0.02 cm^2 V^{-1} s^{-1}) than that with the **DSTQ-14** analogue. These results suggest that the length of thioalkyl side chain

substituents and introduction of the sulfur atom into side moieties have a crucial influence on the charge transport of quinoidal-based n-type organic semiconductors. OFETs based on **DSTQ** derivatives fabricated by conventional spin-coating were also studied in order to compare their charge-transport properties because of the different organic semiconductor deposition techniques. As shown in Figure S7 and summarized in Table 2, the highest mobility extracted from spin-coating (0.064 cm^2 V^{-1} s^{-1} for **DSTQ-14**) is 1 order of magnitude lower than their solution-sheared counterparts. Furthermore, in all cases the mobilities achieved by film spin-coating are always lower than those achieved by solution-shearing, a result correlated to the resulting semiconductor film morphologies as discussed later.

Note, the V_{th} of the solution-shared films are quite large (12−36 V) and larger than those of the spin-coated films (5−15 V). This result is likely due to the large film thickness of the former films (50−80 nm), thus in a top-contact OFET architecture meaning that there is a quite large depletion region which the injected charges have to penetrate before approaching the channel.[65,66] Additional contribution to V_{th} may be due to the crystalline morphology with large grains separated by large grain boundaries. Finally, the high current in the OFF state, thus unoptimal I_{ON}/I_{OFF}s, is again the consequence of the relatively thick semiconducting films in combination with OFET processing in an ambient rather than an N$_2$-filled glove box.

2.5. Thin-Film Microstructural Characterization and Correlation to Charge Transport. To understand the effect of the side chain engineering of the quinoidal compounds on OFETs' performance, thin-film morphologies and molecular packing structures were investigated by polarized optical microscopy (POM, Figure 7), atomic force microscopy
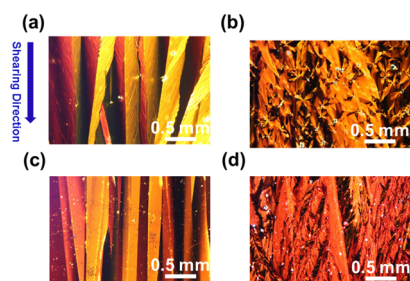
Figure 7. POM image of solution-sheared (a) **DSTQ-6**, (b) **DSTQ-10**, (c) **DSTQ-14**, and (d) **DRTQ-14** thin films.

(AFM, Figure 8), grazing incident X-ray diffraction (GIXRD, Figure 9), and transmission electron microscopy (TEM, Figure S8), using thin films fabricated under the same conditions for OFET active layer fabrication. The POM images of the solution-sheared **DSTQ** films under the cross-polarized light (Figure 7) demonstrate that all films exhibit a crystalline morphology with strong birefringence properties originating from the elongated crystals aligned along the shearing direction. For the solution-sheared **DSTQ-6** films, contiguous millimeter-wide crystalline domains with a length of up to a centimeter are observed, again with crystal plates oriented parallel to the shearing direction. As the thioalkyl side chain length increases from 6 to 10 carbon atoms (thiodecyl), the **DSTQ-10** film shows a different film morphology characterized by spherulitic features with a Maltese cross structure. This morphology features the radial growth of the crystal
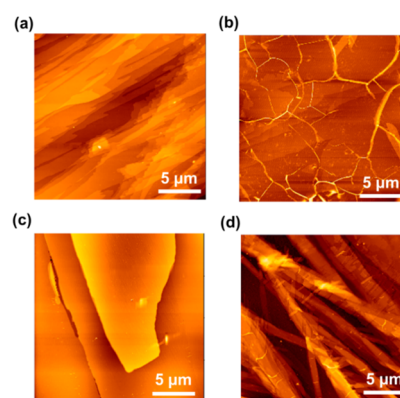
Figure 8. AFM image of solution-sheared (a) **DSTQ-6**, (b) **DSTQ-10**, (c) **DSTQ-14**, and (d) **DRTQ-14** thin films.

domains originating from the nucleation sites, which has been observed for small molecules crystallized in a concentration gradient.[67] Note, a concentration gradient between the bulk solution and the evaporation front also forms during solution-shearing. A different morphology is also observed in **DSTQ-14**, which exhibits a sheet-like morphology with quasi-one-directional continuous crystals. Finally, the **DSTQ-14** films are also textured but visibly more smooth and having fiber-like flakes growing from the larger features when compared to the other **DSTQ**s. These results indicate that the morphology of solution-sheared **DSTQ** films can be significantly influenced by varying the alkyl side chain length.

AFM topographic images of the solution-sheared **DSTQ-6**, **DSTQ-10**, and **DSTQ-14** thin films that possess terrace-like morphologies, whereas **DRTQ-14** exhibits fibrotic features, in agreement with the optical image results. According to the height profile and root-mean-square (rms) roughness (R_{rms}) measurements, by increasing the thioalkyl side chain length the crystal domain size of the **DSTQ** films increases and they become more interconnected. As shown in Figure 8, the film of **DSTQ-14** possesses the largest domain size (∼hundreds of micrometer) and is the smoothest (R_{rms} = 1.9 nm) compared to the other **DSTQ** films. The increased domain size suggests improved thin-film crystallinity, if the domains are well connected as shown for **DSTQ-14**, and it should enhance the charge-carrier mobility. These data are corroborated by the OFET transport parameters shown in Table 2. Interestingly, the **DSTQ-10** film exhibits different correlations between the μ_{max} achieved (0.064 cm^2 V^{-1} s^{-1}) and its R_{rms} value (5.84 nm) with those of the **DSTQ-6** film (μ_{max}: 0.045 cm^2 V^{-1} s^{-1}; R_{rms}: 3.94 nm). This is probably the result of a balance between the crystal size (larger for **DSTQ-10**), domain connectivity by number of grain boundaries (poorer for **DSTQ-6**), and extent of grain boundaries (poorer for **DSTQ-10**). It should be noted that the grain boundaries could create an energy barrier and limit the charge-carrier mobility in organic films. Because of highly ordered layered structures, step heights of 24, 27, 30, and 29 Å can be measured by AFM for **DSTQ-6**, **DSTQ-10**, **DSTQ-14**, and **DRTQ-14** thin films, respectively, along the terrace or fiber topographies. The layered structure heights are in good agreement with the values obtained from 2D GIXRD out-of-plane diffraction patterns, indicating that the film growth packed in a lamellar and out-of-plane fashion (*vide infra*). In addition, the mobility variation between the solution-sheared and spin-coated OFETs is in agreement with the morphologies of the corresponding **DSTQ** films. Thus, spin-
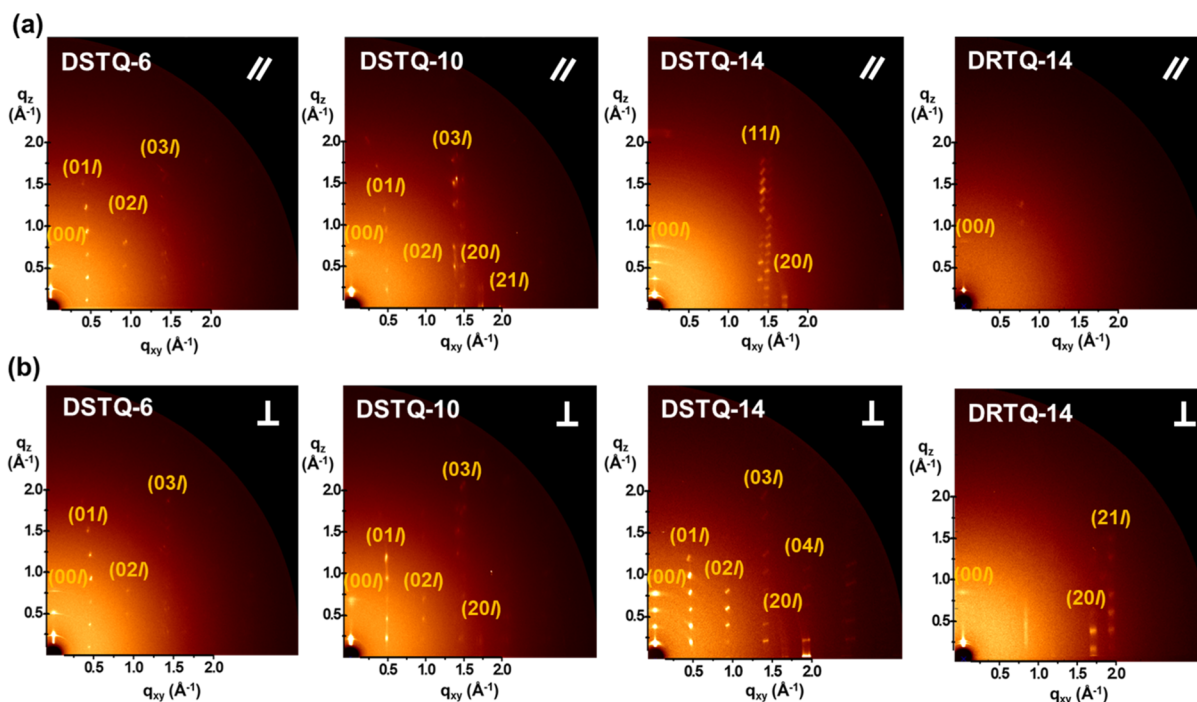
Figure 9. 2D GIXRD patterns of solution-sheared **DSTQ-6**, **DSTQ-10**, **DSTQ-14**, and **DRTQ-14** films with an incident beam along the parallel (∥) and perpendicular (⊥) directions with respect to the shearing direction.

coated **DSTQ** films prepared on the same substrates form much smaller crystals (see POM and AFM images in Figures S9 and S10 of the Supporting Information, respectively), originating from the fast crystal growth process, resulting in a lower field-effect mobility.

2D GIXRD measurements were employed to study the molecular packing and orientation of all solution-sheared films (Figure 9). All of the **DSTQ** films exhibit intense reflections, indicating the presence of crystalline domains. Two kinds of reflection families are observed, the (00l) reflections because of the lamellar layer structure stacking along the q_z direction (out-of-plane) and (hk0) reflections because of the intermolecular packing along the q_{xy} direction (in-plane). By increasing the side chain length, the reflections oriented along the q_z direction become stronger and shift to lower values, thus correlating to the thioalkyl chain length and the molecules packing edge-on with respect to the substrate surface. **DSTQ-14** containing the thiotetradecyl side chain has the largest lamellar spacing (d_{001}) value of 32.19 Å, whereas those for **DSTQ-6** and **DSTQ-10** are 23.85 and 27.50 Å, respectively, in agreement with the shorter chain lengths. **DRTQ-14** exhibits a d_{001}-spacing value of 31.58 Å, which is slightly lower than that of **DSTQ-14**, as a result of the missing sulfur atom in the chain substituent. These results are consistent with the c-axis geometries from X-ray single-crystal diffraction data (Figures 4 and 5) and the alkyl side length value from DFT-optimized geometry calculations (Figure S4). These 2D GIXRD results are also consistent with the AFM height profiles that clearly reflect the layered structure stacked in the lamella stacking. As can be seen in Figure 9, the molecular packing of **DSTQ-14** possesses the sharpest and the highest number of diffraction peaks when compared to **DSTQ-6**, **DSTQ-10**, and **DRTQ-14**, indicating that **DSTQ-14** has the most ordered molecular packing among the solution-sheared **DSTQ** derivatives. The proposed molecular packing of **DSTQ-14** is shown in Figure S11. The

GIXRD patterns with the incident beam parallel and perpendicular to the shearing direction are compared in Figure 9a,b, respectively. **DSTQ-6** and **DSTQ-10** show very similar patterns in these two directions, indicating that the film crystallites are less oriented for the **DSTQ**s with shorter side chains. In contrast, for **DSTQ-14** and **DRTQ-14**, the patterns from the two different beam directions can be clearly distinguished. **DSTQ-14** shows strong (0kl) diffraction peaks in the perpendicular direction but those are absent in the parallel direction; instead, only the (11l) and (20l) reflections appear in the pattern, which implies an oriented microstructure in the film. The highly crystalline, ordered, and oriented packings under shearing conditions are in agreement with the high electron mobility of the solution-sheared **DSTQ-14** films. **DRTQ-14** shows clear (20l) and (21l) peaks in the perpendicular direction, whereas these reflections are rather weak in the parallel direction. Although the solution-sheared **DRTQ-14** film also exhibits orientation under shearing, the overall lower crystallinity reduces **DRTQ-14** carrier mobility versus that of **DSTQ-14**. Regarding the spin-coated films, GIXRD indicates negligible diffraction features (Figure S12), thus indicating poor texturing and absence of preferential molecular alignment. These experimental results are in agreement with the charge transport data.

Furthermore, as shown by the TEM images (Figure S8a,c), the crystal growth in solution-sheared **DSTQ-14** thin films exhibits a smoother surface than that of **DRTQ-14**. In addition, the electron diffraction (Figure S8b,d) patterns show that the thin film of **DSTQ-14** produces sharp and well-defined diffractions, whereas the thin film of **DRTQ-14** gives less and ill-defined diffraction spots, indicating that **DSTQ-14** molecules pack into more ordered domains than **DRTQ-14**. This result probably originates from the S(alkyl)···S-(thiophene) intramolecular lock that greatly planarizes the core in **DSTQ-14**, resulting in a low torsion angle (2.71°),

which promotes intermolecular interactions and crystallization. On the other hand, when there is no sulfur in the side moiety as in **DRTQ-14**, the larger steric demand of the long hydrocarbon chains results in a larger torsional angle in **DRTQ-14** (5.17°), in agreement with other studies.[68−70] Thus, core distortion, molecular packing, and degree of order in thin films can be effectively altered by the introduction of the sulfur atom in the alkyl moieties.

2.6. Device Stability Measurements. The long-term environmental stability of **DSTQ** OFETs was investigated by monitoring the electron mobility after device storage for over 30 days in air (controlled relative humidity of 45−55%). As shown in Figure S13, all the nonencapsulated **DSTQ** OFETs based on silver electrodes do not degrade significantly after storage. Their good air stability indicates that **DSTQ**s have great potential as low-cost and air-stable n-channel OFETs. This property was obtained because of the contribution of two strong electron-withdrawing groups attached to the π-conjugated **DSTQ** backbone that lowers the LUMO energy level down to −4.28 eV and tight molecular packing preventing diffusion of ambient-containing electron traps. After storage for over 30 days, the stability of **DSTQ-14** OFETs to electrical stress was further investigated by subjecting them to a continuous V_g sweeping (−40 V < V_g < 80 V) under a constant V_d of 80 V (Figure S14). After scans of 100 cycles, only a slight increase of the channel current was observed, indicating that **DSTQ** compounds can sustain charge transport in ambient without significant trap-induced deterioration upon bias stress.

3. CONCLUSIONS

In conclusion, we have developed a new π-conjugated quinoidal **DSTQ** series for OFETs. Introduction of thioalkyl substituents with different chain lengths has been investigated for these compounds in order to establish molecular structure, morphology, molecular packing and OFET performance relationships. It was found that longer side chains improve solubility for efficient thin-film processing using the solution-shearing method as well as molecular packing and charge-transport characteristics. In addition, sulfur atom introduction in between the π-core and the alkyl side chain has also a great impact on the electronic structure, surface morphology, as well as solid-state molecular packing, resulting in a narrower band gap, lower LUMO energy level, as well as more interconnected semiconductor domains. These properties favorably impact electron transport and these observations are reinforced by optical absorption, microscopic images, TEM, and GIXRD measurements. Among the **DSTQ** derivatives, solution-sheared **DSTQ-14** possesses the highest mobility of up to 0.77 cm² V⁻¹ s⁻¹, good ambient and electrical stability, thus making it a promising new solution-processable and air-stable organic semiconductor for OFET applications.

4. EXPERIMENTAL SECTION

4.1. Material Synthesis. All the chemical reagents were purchased from Aldrich, Alfa, and TCI Chemical Co. and used as received unless otherwise noted. Solvents for reactions (toluene and THF) were distilled under nitrogen from sodium/benzophenone ketyl, and halogenated solvents were distilled from CaH₂. Silane agent for the self-assembly monolayer treatment, (2-phenylethyl)-trichlorosilane or octyltrichlorosilane, was obtained from Gelest, Inc.

4.2. General Procedures for Final Compounds (1−4). Malononitrile (1.2 mmol) was added to a solution of sodium hydride

(2.4 mmol) in dry dimethoxyethane (30 mL) at 0 °C. After addition, the reaction mixture was warmed to room temperature and stirred for 20 min. Next, compound (**10a−d**) (0.3 mmol) and tetrakis(triphenyl-phosphine)palladium (0.09 mmol) were added to the reaction mixture. The mixture was refluxed for 6 h, and then it was quenched with saturated bromine water at 0 °C and stirred for 15 min. The mixture was extracted with CH₂Cl₂, washed with brine, dried over Na₂SO₄, and evaporated. The residue was purified by column chromatography using CH₂Cl₂/hexanes (1:1).

4.2.1. Synthesis of DSTQ-6 (1). The title compound was obtained as a dark green solid (yield = 38%). mp 194 °C. ¹H NMR (500 MHz, CDCl₃): δ 7.59 (d, J = 5.6 Hz, 2 H), 7.41 (d, J = 5.5 Hz, 2 H), 3.07 (t, J = 7.3 Hz, 4 H), 1.69−1.62 (m, 4 H), 1.46−1.41 (m, 4 H), 1.22−1.32 (m, 40 H), 0.88 (t, J = 7.0 Hz, 6 H). ¹³C NMR (125 MHz, CDCl₃): δ 171.88, 150.76, 141.98, 140.01, 135.54, 131.74, 113.83, 113.29, 69.63, 38.27, 31.23, 29.62, 28.43, 22.48, 13.98. HRMS (m/z: FAB⁺) calcd for C₃₀H₃₀N₄S₅, 606.1074; found, 606.1076.

4.2.2. Synthesis of DRTQ-10 (2). The title compound was obtained as a dark blue solid (yield = 48%). mp 195 °C. ¹H NMR (500 MHz, CDCl₃): δ 7.56 (d, J = 5.0 Hz, 2 H), 7.37 (d, J = 5.5 Hz, 2 H), 3.05 (t, J = 7.0 Hz, 4 H), 1.68−1.64 (m, 4 H), 1.44−1.38 (m, 4 H), 1.22−1.29 (m, 24 H), 0.86 (t, J = 7.0 Hz, 6 H). ¹³C NMR (125 MHz, CDCl₃): δ 171.88, 150.75, 142.00, 140.03, 135.53, 131.71, 113.81, 113.29, 69.59, 38.22, 31.88, 29.66, 29.51, 29.46, 29.29, 29.06, 28.75, 22.68, 14.11. HRMS (m/z: FAB⁺) calcd for C₃₈H₄₆N₄S₅, 718.2326; found, 718.2330.

4.2.3. Synthesis of DSTQ-14 (3). The title compound was obtained as a dark green solid (yield = 38%). mp 198 °C. ¹H NMR (500 MHz, CDCl₃): δ 7.55 (d, J = 5.5 Hz, 2 H), 7.37 (d, J = 5.5 Hz, 2 H), 3.03 (t, J = 7.0 Hz, 4 H), 1.65−1.62 (m, 4 H), 1.42−1.38 (m, 4 H), 1.23−1.28 (m, 40 H), 0.86 (t, J = 7.0 Hz, 6 H). ¹³C NMR (125 MHz, CDCl₃): δ 171.86, 150.74, 141.97, 139.99, 135.53, 131.72, 113.82, 113.28, 69.64, 38.23, 31.92, 29.67, 29.48, 29.36, 29.08, 28.77, 22.69, 14.12. HRMS (m/z: FAB⁺) calcd for C₄₆H₆₂N₄S₅, 830.3578; found, 830.3578.

4.2.4. Synthesis of DRTQ-14 (4). The title compound was obtained as a dark blue solid (yield = 48%). mp 192 °C. ¹H NMR (500 MHz, CDCl₃): δ 7.56 (d, J = 5.5 Hz, 2 H), 7.31 (d, J = 5.0 Hz, 2 H), 2.82−2.75 (b, 4 H), 1.42−1.21 (m, 48 H), 0.88 (t, J = 7.0 Hz, 6 H). ¹³C NMR (125 MHz, CDCl₃): δ 170.83, 151.09, 143.24, 140.85, 136.94, 130.60, 113.82, 113.15, 68.30, 31.92, 30.88, 29.81, 29.66, 29.59, 29.48, 29.35, 29.23, 29.13, 22.68, 14.09. HRMS (m/z: FAB⁺) calcd for C₄₆H₆₂N₄S₃, 766.4137; found, 766.4135.

■ ASSOCIATED CONTENT

Ⓢ Supporting Information

The Supporting Information is available free of charge at https://pubs.acs.org/doi/10.1021/acsami.0c03477.

> Synthetic details of all compounds; DSC; TGA; DFT-derived HOMOs and LUMOs; single-crystal structures of **DSTQ-14** and **DRTQ-14**; transfer characteristics; POM images; AFM images; TEM images; ambient stability; electrical stability measurements; and NMR spectra (PDF)

> Crystallographic data of DSTQ-14 (CIF)

> Crystallographic data of DRTQ-14 (CIF)

■ AUTHOR INFORMATION

Corresponding Authors

Cheng-Liang Liu − *Department of Chemical and Materials Engineering and Research Center of New Generation Light Driven Photovoltaic Module, National Central University, Taoyuan 32001, Taiwan;* ⓞ orcid.org/0000-0002-8778-5386; Email: clliu@ncu.edu.tw

Ming-Chou Chen − *Department of Chemistry and Research Center of New Generation Light Driven Photovoltaic Module,*

National Central University, Taoyuan 32001, Taiwan;
 orcid.org/0000-0001-9033-0131; Email: mcchen@
ncu.edu.tw

Antonio Facchetti − *Department of Chemistry, Northwestern University, Evanston, Illinois 60208, United States;*
 orcid.org/0000-0002-8175-7958; Email: a-facchetti@
northwestern.edu

Authors

  Sureshraju Vegiraju − *Department of Chemistry and Research Center of New Generation Light Driven Photovoltaic Module, National Central University, Taoyuan 32001, Taiwan*

  Alfonsina Abat Amelenan Torimtubun − *Department of Chemical and Materials Engineering and Research Center of New Generation Light Driven Photovoltaic Module, National Central University, Taoyuan 32001, Taiwan*

  Po-Shen Lin − *Department of Chemical and Materials Engineering and Research Center of New Generation Light Driven Photovoltaic Module, National Central University, Taoyuan 32001, Taiwan*

  Hsin-Chia Tsai − *Department of Chemistry and Research Center of New Generation Light Driven Photovoltaic Module, National Central University, Taoyuan 32001, Taiwan*

  Wei-Chieh Lien − *Department of Chemistry and Research Center of New Generation Light Driven Photovoltaic Module, National Central University, Taoyuan 32001, Taiwan*

  Cheng-Shiun Chen − *Department of Chemistry and Research Center of New Generation Light Driven Photovoltaic Module, National Central University, Taoyuan 32001, Taiwan*

  Guan-Yu He − *Department of Chemical and Materials Engineering and Research Center of New Generation Light Driven Photovoltaic Module, National Central University, Taoyuan 32001, Taiwan*

  Chih-Yu Lin − *Department of Chemical and Materials Engineering and Research Center of New Generation Light Driven Photovoltaic Module, National Central University, Taoyuan 32001, Taiwan*

  Ding Zheng − *Department of Chemistry, Northwestern University, Evanston, Illinois 60208, United States*

  Yi-Fan Huang − *Department of Applied Chemistry, National Chiao Tung University, Hsinchu 30010, Taiwan*

  Yi-Ching Wu − *Department of Chemistry and Research Center of New Generation Light Driven Photovoltaic Module, National Central University, Taoyuan 32001, Taiwan*

  Shueh-Lin Yau − *Department of Chemistry and Research Center of New Generation Light Driven Photovoltaic Module, National Central University, Taoyuan 32001, Taiwan*

  Gene-Hsiang Lee − *Instrumentation Center, National Taiwan University, Taipei 10617, Taiwan*

  Shih-Huang Tung − *Institute of Polymer Science and Engineering, National Taiwan University, Taipei 10617, Taiwan;* orcid.org/0000-0002-6787-4955

  Chien-Lung Wang − *Department of Applied Chemistry, National Chiao Tung University, Hsinchu 30010, Taiwan;*
 orcid.org/0000-0002-5977-2836

Complete contact information is available at:
https://pubs.acs.org/10.1021/acsami.0c03477

Author Contributions

¶S.V. and A.A.A.T. contributed equally to this work.

Notes

The authors declare no competing financial interest.

REFERENCES

(1) Di, C.-a.; Shen, H.; Zhang, F.; Zhu, D. Enabling Multifunctional Organic Transistors with Fine-Tuned Charge Transport. *Acc. Chem. Res.* **2019**, *52*, 1113−1124.

(2) Wang, N.; Yang, A.; Fu, Y.; Li, Y.; Yan, F. Functionalized Organic Thin Film Transistors for Biosensing. *Acc. Chem. Res.* **2019**, *52*, 277−287.

(3) Lee, M. Y.; Lee, H. R.; Park, C. H.; Han, S. G.; Oh, J. H. Organic Transistor-Based Chemical Sensors for Wearable Bioelectronics. *Acc. Chem. Res.* **2018**, *51*, 2829−2838.

(4) Zhang, X.; Dong, H.; Hu, W. Organic Semiconductor Single Crystals for Electronics and Photonics. *Adv. Mater.* **2018**, *30*, 1801048.

(5) Zeglio, E.; Inganäs, O. Active Materials for Organic Electrochemical Transistors. *Adv. Mater.* **2018**, *30*, 1800941.

(6) Wu, X.; Mao, S.; Chen, J.; Huang, J. Strategies for Improving the Performance of Sensors Based on Organic Field-Effect Transistors. *Adv. Mater.* **2018**, *30*, 1705642.

(7) Wu, J.; Li, Q.; Xue, G.; Chen, H.; Li, H. Preparation of Single-Crystalline Heterojunctions for Organic Electronics. *Adv. Mater.* **2017**, *29*, 1606101.

(8) Li, H.; Shi, W.; Song, J.; Jang, H.-J.; Dailey, J.; Yu, J.; Katz, H. E. Chemical and Biomolecule Sensing with Organic Field-Effect Transistors. *Chem. Rev.* **2019**, *119*, 3−35.

(9) Kang, B.; Lee, W. H.; Cho, K. Recent Advances in Organic Transistor Printing Processes. *ACS Appl. Mater. Interfaces* **2013**, *5*, 2302−2315.

(10) Takimiya, K.; Osaka, I.; Mori, T.; Nakano, M. Organic Semiconductors Based on [1]Benzothieno[3,2-b][1]benzothiophene Substructure. *Acc. Chem. Res.* **2014**, *47*, 1493−1502.

(11) Yang, J.; Zhao, Z.; Wang, S.; Guo, Y.; Liu, Y. Insight into High-Performance Conjugated Polymers for Organic Field-Effect Transistors. *Chem* **2018**, *4*, 2748−2785.

(12) Paterson, A. F.; Singh, S.; Fallon, K. J.; Hodsden, T.; Han, Y.; Schroeder, B. C.; Bronstein, H.; Heeney, M.; McCulloch, I.; Anthopoulos, T. D. Recent Progress in High-Mobility Organic Transistors: A Reality Check. *Adv. Mater.* **2018**, *30*, 1801079.

(13) Zhang, J.; Jin, J.; Xu, H.; Zhang, Q.; Huang, W. Recent Progress on Organic Donor−Acceptor Complexes as Active Elements in Organic Field-Effect Transistors. *J. Mater. Chem. C* **2018**, *6*, 3485−3498.

(14) Kang, B.; Ge, F.; Qiu, L.; Cho, K. Effective Use of Electrically Insulating Units in Organic Semiconductor Thin Films for High-Performance Organic Transistors. *Adv. Electron. Mater.* **2017**, *3*, 1600240.

(15) Liu, Z.; Zhang, G.; Zhang, D. Modification of Side Chains of Conjugated Molecules and Polymers for Charge Mobility Enhancement and Sensing Functionality. *Acc. Chem. Res.* **2018**, *51*, 1422−1432.

(16) Naibi Lakshminarayana, A.; Ong, A.; Chi, C. Modification of Acenes for n-Channel OFET Materials. *J. Mater. Chem. C* **2018**, *6*, 3551−3563.

(17) Quinn, J. T. E.; Zhu, J.; Li, X.; Wang, J.; Li, Y. Recent Progress in the Development of n-Type Organic Semiconductors for Organic Field Effect Transistors. *J. Mater. Chem. C* **2017**, *5*, 8654−8681.

(18) Sun, H.; Gerasimov, J.; Berggren, M.; Fabiano, S. n-Type organic electrochemical transistors: materials and challenges. *J. Mater. Chem. C* **2018**, *6*, 11778−11784.

(19) Zhao, Y.; Guo, Y.; Liu, Y. 25th Anniversary Article: Recent Advances in n-Type and Ambipolar Organic Field-Effect Transistors. *Adv. Mater.* **2013**, *25*, 5372−5391.

(20) Qiao, Y.; Guo, Y.; Yu, C.; Zhang, F.; Xu, W.; Liu, Y.; Zhu, D. Diketopyrrolopyrrole-Containing Quinoidal Small Molecules for High-Performance, Air-Stable, and Solution-Processable n-Channel Organic Field-Effect Transistors. *J. Am. Chem. Soc.* **2012**, *134*, 4084−4087.

(21) Zhou, N.; Vegiraju, S.; Yu, X.; Manley, E. F.; Butler, M. R.; Leonardi, M. J.; Guo, P.; Zhao, W.; Hu, Y.; Prabakaran, K.; Chang, R. P. H.; Ratner, M. A.; Chen, L. X.; Facchetti, A.; Chen, M.-C.; Marks, T. J. Diketopyrrolopyrrole (DPP) Functionalized Tetrathienothiophene (TTA) Small Molecules for Organic Thin Film Transistors and Photovoltaic Cells. *J. Mater. Chem. C* **2015**, *3*, 8932−8941.

(22) Würthner, F.; Stolte, M. Naphthalene and Perylene Diimides for Organic Transistors. *Chem. Commun.* **2011**, *47*, 5109−5115.

(23) Guo, X.; Kim, F. S.; Seger, M. J.; Jenekhe, S. A.; Watson, M. D. Naphthalene Diimide-Based Polymer Semiconductors: Synthesis, Structure−Property Correlations, and n-Channel and Ambipolar Field-Effect Transistors. *Chem. Mater.* **2012**, *24*, 1434−1442.

(24) Wang, S.; Sun, H.; Erdmann, T.; Wang, G.; Fazzi, D.; Lappan, U.; Puttisong, Y.; Chen, Z.; Berggren, M.; Crispin, X.; Kiriy, A.; Voit, B.; Marks, T. J.; Fabiano, S.; Facchetti, A. A Chemically Doped Naphthalenediimide-Bithiazole Polymer for n-Type Organic Thermoelectrics. *Adv. Mater.* **2018**, *30*, 1801898.

(25) Chen, H. Z.; Ling, M. M.; Mo, X.; Shi, M. M.; Wang, M.; Bao, Z. Air Stable n-Channel Organic Semiconductors for Thin Film Transistors Based on Fluorinated Derivatives of Perylene Diimides. *Chem. Mater.* **2007**, *19*, 816−824.

(26) Youn, J.; Huang, P.-Y.; Huang, Y.-W.; Chen, M.-C.; Lin, Y.-J.; Huang, H.; Ortiz, R. P.; Stern, C.; Chung, M.-C.; Feng, C.-Y.; Chen, L.-H.; Facchetti, A.; Marks, T. J. Versatile *α,ω*-Disubstituted Tetrathienoacene Semiconductors for High Performance Organic Thin-Film Transistors. *Adv. Funct. Mater.* **2012**, *22*, 48−60.

(27) Wu, Q.; Li, R.; Hong, W.; Li, H.; Gao, X.; Zhu, D. Dicyanomethylene-Substituted Fused Tetrathienoquinoid for High-Performance, Ambient-Stable, Solution-Processable n-Channel Organic Thin-Film Transistors. *Chem. Mater.* **2011**, *23*, 3138−3140.

(28) Marrocchi, A.; Facchetti, A.; Lanari, D.; Petrucci, C.; Vaccaro, L. Current Methodologies for a Sustainable Approach to *π*-Conjugated Organic Semiconductors. *Energy Environ. Sci.* **2016**, *9*, 763−786.

(29) Yoon, M.-H.; Facchetti, A.; Stern, C. E.; Marks, T. J. Fluorocarbon-Modified Organic Semiconductors: Molecular Architecture, Electronic, and Crystal Structure Tuning of Arene- versus Fluoroarene-Thiophene Oligomer Thin-Film Properties. *J. Am. Chem. Soc.* **2006**, *128*, 5792−5801.

(30) Huang, D.; Yao, H.; Cui, Y.; Zou, Y.; Zhang, F.; Wang, C.; Shen, H.; Jin, W.; Zhu, J.; Diao, Y.; Xu, W.; Di, C.-a.; Zhu, D. Conjugated-Backbone Effect of Organic Small Molecules for n-Type Thermoelectric Materials with ZT over 0.2. *J. Am. Chem. Soc.* **2017**, *139*, 13013−13023.

(31) Suzuki, Y.; Miyazaki, E.; Takimiya, K. ((Alkyloxy)carbonyl)-cyanomethylene-Substituted Thienoquinoidal Compounds: a New Class of Soluble n-Channel Organic Semiconductors for Air-Stable Organic Field-Effect Transistors. *J. Am. Chem. Soc.* **2010**, *132*, 10453−10466.

(32) Chesterfield, R. J.; Newman, C. R.; Pappenfus, T. M.; Ewbank, P. C.; Haukaas, M. H.; Mann, K. R.; Miller, L. L.; Frisbie, C. D. High Electron Mobility and Ambipolar Transport in Organic Thin-Film Transistors Based on a *π*-Stacking Quinoidal Terthiophene. *Adv. Mater.* **2003**, *15*, 1278−1282.

(33) Janzen, D. E.; Burand, M. W.; Ewbank, P. C.; Pappenfus, T. M.; Higuchi, H.; da Silva Filho, D. A.; Young, V. G.; Brédas, J.-L.; Mann, K. R. Preparation and Characterization of *π*-Stacking Quinodimethane Oligothiophenes. Predicting Semiconductor Behavior and

Bandwidths from Crystal Structures and Molecular Orbital Calculations. *J. Am. Chem. Soc.* **2004**, *126*, 15295−15308.

(34) Handa, S.; Miyazaki, E.; Takimiya, K.; Kunugi, Y. Solution-Processable n-Channel Organic Field-Effect Transistors Based on Dicyanomethylene-Substituted Terthienoquinoid Derivative. *J. Am. Chem. Soc.* **2007**, *129*, 11684−11685.

(35) Pappenfus, T. M.; Chesterfield, R. J.; Frisbie, C. D.; Mann, K. R.; Casado, J.; Raff, J. D.; Miller, L. L. A *π*-Stacking Terthiophene-Based Quinodimethane Is an n-Channel Conductor in a Thin Film Transistor. *J. Am. Chem. Soc.* **2002**, *124*, 4184−4185.

(36) Kawabata, K.; Saito, M.; Osaka, I.; Takimiya, K. Very Small Bandgap *π*-Conjugated Polymers with Extended Thienoquinoids. *J. Am. Chem. Soc.* **2016**, *138*, 7725−7732.

(37) Mori, T.; Yanai, N.; Osaka, I.; Takimiya, K. Quinoidal Naphtho[1,2-b:5,6-b′]dithiophenes for Solution-Processed n-Channel Organic Field-Effect Transistors. *Org. Lett.* **2014**, *16*, 1334−1337.

(38) Vegiraju, S.; He, G.-Y.; Kim, C.; Priyanka, P.; Chiu, Y.-J.; Liu, C.-W.; Huang, C.-Y.; Ni, J.-S.; Wu, Y.-W.; Chen, Z.; Lee, G.-H.; Tung, S.-H.; Liu, C.-L.; Chen, M.-C.; Facchetti, A. Solution-Processable Dithienothiophenoquinoid (DTTQ) Structures for Ambient-Stable n-Channel Organic Field Effect Transistors. *Adv. Funct. Mater.* **2017**, *27*, 1606761.

(39) Zhang, C.; Zang, Y.; Zhang, F.; Diao, Y.; McNeill, C. R.; Di, C.-a.; Zhu, X.; Zhu, D. Pursuing High-Mobility n-Type Organic Semiconductors by Combination of "Molecule-Framework" and "Side-Chain" Engineering. *Adv. Mater.* **2016**, *28*, 8456−8462.

(40) Ribierre, J. C.; Tanaka, T.; Zhao, L.; Yokota, Y.; Matsumoto, S.; Hashizume, D.; Takaishi, K.; Muto, T.; Heinrich, B.; Méry, S.; Mathevet, F.; Matsushima, T.; Uchiyama, M.; Adachi, C.; Aoyama, T. Simultaneous Edge-on to Face-on Reorientation and 1D Alignment of Small *π*-Conjugated Molecules Using Room-Temperature Mechanical Rubbing. *Adv. Funct. Mater.* **2018**, *28*, 1707038.

(41) Wu, H.; Wang, Y.; Qiao, X.; Wang, D.; Yang, X.; Li, H. Pyrrolo[3,2-b]pyrrole-Based Quinoidal Compounds For High Performance n-Channel Organic Field-Effect Transistor. *Chem. Mater.* **2018**, *30*, 6992−6997.

(42) Ren, L.; Yuan, D.; Gann, E.; Guo, Y.; Thomsen, L.; McNeill, C. R.; Di, C.-a.; Yi, Y.; Zhu, X.; Zhu, D. Critical Role of Molecular Symmetry for Charge Transport Properties: A Paradigm Learned from Quinoidal Bithieno[3,4-b]thiophenes. *Chem. Mater.* **2017**, *29*, 4999−5008.

(43) Hu, Y.; Berdunov, N.; Di, C.-a.; Nandhakumar, I.; Zhang, F.; Gao, X.; Zhu, D.; Sirringhaus, H. Effect of Molecular Asymmetry on the Charge Transport Physics of High Mobility n-Type Molecular Semiconductors Investigated by Scanning Kelvin Probe Microscopy. *ACS Nano* **2014**, *8*, 6778−6787.

(44) Xiong, Y.; Tao, J.; Wang, R.; Qiao, X.; Yang, X.; Wang, D.; Wu, H.; Li, H. A Furan−Thiophene-Based Quinoidal Compound: A New Class of Solution-Processable High-Performance n-Type Organic Semiconductor. *Adv. Mater.* **2016**, *28*, 5949−5953.

(45) Cui, C.; Wong, W.-Y.; Li, Y. Improvement of Open-Circuit Voltage and Photovoltaic Properties of 2D-Conjugated Polymers by Alkylthio Substitution. *Energy Environ. Sci.* **2014**, *7*, 2276−2284.

(46) Hou, J.; Fan, B.; Huo, L.; He, C.; Yang, C.; Li, Y. Poly(alkylthio-p-phenylenevinylene): Synthesis and Electroluminescent and Photovoltaic Properties. *J. Polym. Sci., Part A: Polym. Chem.* **2006**, *44*, 1279−1290.

(47) Cui, C.; Guo, X.; Min, J.; Guo, B.; Cheng, X.; Zhang, M.; Brabec, C. J.; Li, Y. High-Performance Organic Solar Cells Based on a Small Molecule with Alkylthio-Thienyl-Conjugated Side Chains without Extra Treatments. *Adv. Mater.* **2015**, *27*, 7469−7475.

(48) Vegiraju, S.; Chang, B.-C.; Priyanka, P.; Huang, D.-Y.; Wu, K.-Y.; Li, L.-H.; Chang, W.-C.; Lai, Y.-Y.; Hong, S.-H.; Yu, B.-C.; Wang, C.-L.; Chang, W.-J.; Liu, C.-L.; Chen, M.-C.; Facchetti, A. Intramolecular Locked Dithioalkylbithiophene-Based Semiconductors for High-Performance Organic Field-Effect Transistors. *Adv. Mater.* **2017**, *29*, 1702414.

(49) Di Maria, F.; Olivelli, P.; Gazzano, M.; Zanelli, A.; Biasiucci, M.; Gigli, G.; Gentili, D.; D'Angelo, P.; Cavallini, M.; Barbarella, G. A

Successful Chemical Strategy To Induce Oligothiophene Self-Assembly into Fibers with Tunable Shape and Function. *J. Am. Chem. Soc.* **2011**, *133*, 8654−8661.

(50) Huang, H.; Yang, L.; Facchetti, A.; Marks, T. J. Organic and Polymeric Semiconductors Enhanced by Noncovalent Conformational Locks. *Chem. Rev.* **2017**, *117*, 10291−10318.

(51) Vegiraju, S.; Luo, X.-L.; Li, L.-H.; Afraj, S. N.; Lee, C.; Zheng, D.; Hsieh, H.-C.; Lin, C.-C.; Hong, S.-H.; Tsai, H.-C.; Lee, G.-H.; Tung, S.-H.; Liu, C.-L.; Chen, M.-C.; Facchetti, A. Solution Processable Pseudo n-Thienoacenes via Intramolecular S⋯S Lock for High Performance Organic Field Effect Transistors. *Chem. Mater.* **2020**, *32*, 1422−1429.

(52) Prasanthkumar, S.; Saeki, A.; Seki, S.; Ajayaghosh, A. Solution Phase Epitaxial Self-Assembly and High Charge-Carrier Mobility Nanofibers of Semiconducting Molecular Gelators. *J. Am. Chem. Soc.* **2010**, *132*, 8866−8867.

(53) Musser, A. J.; Rajendran, S. K.; Georgiou, K.; Gai, L.; Grant, R. T.; Shen, Z.; Cavazzini, M.; Ruseckas, A.; Turnbull, G. A.; Samuel, I. D. W.; Clark, J.; Lidzey, D. G. Intermolecular States in Organic Dye Dispersions: Excimers vs. Aggregates. *J. Mater. Chem. C* **2017**, *5*, 8380−8389.

(54) Böckmann, M.; Schemme, T.; de Jong, D. H.; Denz, C.; Heuer, A.; Doltsinis, N. L. Structure of P3HT Crystals, Thin Films, and Solutions by UV/Vis Spectral Analysis. *Phys. Chem. Chem. Phys.* **2015**, *17*, 28616−28625.

(55) Hestand, N. J.; Spano, F. C. Molecular Aggregate Photophysics beyond the Kasha Model: Novel Design Principles for Organic Materials. *Acc. Chem. Res.* **2017**, *50*, 341−350.

(56) Hwang, H.; Khim, D.; Yun, J.-M.; Jung, E.; Jang, S.-Y.; Jang, Y. H.; Noh, Y.-Y.; Kim, D.-Y. Quinoidal Molecules as a New Class of Ambipolar Semiconductor Originating from Amphoteric Redox Behavior. *Adv. Funct. Mater.* **2015**, *25*, 1146−1156.

(57) Moliton, A.; Hiorns, R. C. Review of Electronic and Optical Properties of Semiconducting π-Conjugated Polymers: Applications in Optoelectronics. *Polym. Int.* **2004**, *53*, 1397−1412.

(58) Chen, M.-C.; Kim, C.; Chen, S.-Y.; Chiang, Y.-J.; Chung, M.-C.; Facchetti, A.; Marks, T. J. Functionalized Anthradithiophenes for Organic Field-Effect Transistors. *J. Mater. Chem.* **2008**, *18*, 1029−1036.

(59) Gu, X.; Shaw, L.; Gu, K.; Toney, M. F.; Bao, Z. The Meniscus-Guided Deposition of Semiconducting Polymers. *Nat. Commun.* **2018**, *9*, 534.

(60) Khim, D.; Luzio, A.; Bonacchini, G. E.; Pace, G.; Lee, M.-J.; Noh, Y.-Y.; Caironi, M. Uniaxial Alignment of Conjugated Polymer Films for High-Performance Organic Field-Effect Transistors. *Adv. Mater.* **2018**, *30*, 1705463.

(61) Qu, G.; Kwok, J. J.; Mohammadi, E.; Zhang, F.; Diao, Y. Understanding Film-To-Stripe Transition of Conjugated Polymers Driven by Meniscus Instability. *ACS Appl. Mater. Interfaces* **2018**, *10*, 40692−40701.

(62) Zhou, Z.; Zhang, Z.; Wu, Q.; Ji, X.; Wang, J.; Zeng, X.; Feng, S.-P.; Chan, P. K. L. Inch-Scale Grain Boundary Free Organic Crystals Developed by Nucleation Seed-Controlled Shearing Method. *ACS Appl. Mater. Interfaces* **2018**, *10*, 35395−35403.

(63) Horstman, E. M.; Kafle, P.; Zhang, F.; Zhang, Y.; Kenis, P. J. A.; Diao, Y. Solution Coating of Pharmaceutical Nanothin Films and Multilayer Nanocomposites with Controlled Morphology and Polymorphism. *ACS Appl. Mater. Interfaces* **2018**, *10*, 10480−10489.

(64) Molina-Lopez, F.; Yan, H.; Gu, X.; Kim, Y.; Toney, M. F.; Bao, Z. Electric Field Tuning Molecular Packing and Electrical Properties of Solution-Shearing Coated Organic Semiconducting Thin Films. *Adv. Funct. Mater.* **2017**, *27*, 1605503.

(65) Pfattner, R.; Rovira, C.; Mas-Torrent, M. Organic metal engineering for enhanced field-effect transistor performance. *Phys. Chem. Chem. Phys.* **2015**, *17*, 26545−26552.

(66) Schroeder, R.; Majewski, L. A.; Grell, M. A Study of the Threshold Voltage in Pentacene Organic Field-Effect Transistors. *Appl. Phys. Lett.* **2003**, *83*, 3201−3203.

(67) Rogowski, R. Z.; Darhuber, A. A. Crystal Growth near Moving Contact Lines on Homogeneous and Chemically Patterned Surfaces. *Langmuir* **2010**, *26*, 11485−11493.

(68) Wang, K.; Liu, W.; Zheng, C.-J.; Shi, Y.-Z.; Liang, K.; Zhang, M.; Ou, X.-M.; Zhang, X.-H. A Comparative Study of Carbazole-Based Thermally Activated Delayed Fluorescence Emitters with Different Steric Hindrance. *J. Mater. Chem. C* **2017**, *5*, 4797−4803.

(69) Yuan, M.; Tanabe, I.; Bernard-Schaaf, J.-M.; Shi, Q.-Y.; Schlegel, V.; Schurhammer, R.; Dowben, P. A.; Doudin, B.; Routaboul, L.; Braunstein, P. Influence of Steric Hindrance on the Molecular Packing and the Anchoring of Quinonoid Zwitterions on Gold Surfaces. *New J. Chem.* **2016**, *40*, 5782−5796.

(70) Maxwell, P. I.; Popelier, P. L. A. Unfavorable regions in the ramachandran plot: Is it Really Steric Hindrance? The Interacting Quantum Atoms Perspective. *J. Comput. Chem.* **2017**, *38*, 2459−2474.